



Contents lists available at ScienceDirect

Journal of the Mechanics and Physics of Solids

journal homepage: www.elsevier.com/locate/jmps

A single degree of freedom ‘lollipop’ model for carbon nanotube bundle formation

Steven Cranford^{a,b}, Haimin Yao^{b,c}, Christine Ortiz^{b,c}, Markus J. Buehler^{a,b,*}

^a Laboratory for Atomistic and Molecular Mechanics, Department of Civil and Environmental Engineering, Massachusetts Institute of Technology, 77 Massachusetts Ave. Room 1-235A&B, Cambridge, MA, USA

^b Center for Materials Science and Engineering, Massachusetts Institute of Technology, 77 Massachusetts Ave., Cambridge, MA, USA

^c Department of Materials Science and Engineering, Massachusetts Institute of Technology, 77 Massachusetts Ave., Cambridge, MA, USA

ARTICLE INFO

Article history:

Received 21 July 2009

Received in revised form

8 October 2009

Accepted 4 November 2009

Keywords:

Carbon nanotubes

Adhesion

van der Waals interactions

Mesoscale

Self-assembly

ABSTRACT

Current carbon nanotube (CNT) synthesis methods include the production of ordered, free-standing vertically aligned arrays, the properties of which are partially governed by interactions between adjacent tubes. Using material parameters determined by atomistic methods, here we represent individual CNTs by a simple single degree of freedom ‘lollipop’ model to investigate the formation, mechanics, and self-organization of CNT bundles driven by weak van der Waals interactions. The computationally efficient simple single degree of freedom model enables us to study arrays consisting of hundreds of thousands of nanotubes. The effects of nanotube parameters such as aspect ratio, bending stiffness, and surface energy, on formation and bundle size, as well as the intentional manipulation of bundle pattern formation, are investigated. We report studies with both single wall carbon nanotubes (SWCNTs) and double wall carbon nanotubes (DWCNTs) with varying aspect ratios (that is, varying height). We calculate the local density distributions of the nanotube bundles and show that there exists a maximum attainable bundle density regardless of an increase in surface energy for nanotubes with given spacing and stiffness. In addition to applications to CNTs, our model can also be applied to other types of nanotube arrays (e.g. protein nanotubes, polymer nanofilaments).

© 2009 Elsevier Ltd. All rights reserved.

1. Introduction

Carbon nanotubes are among the most widely studied nanomaterials, with many potential applications that take advantage of their unique mechanical, electrical, thermal, and optical properties (Baughman et al., 2002). There are many concurrent investigations involving carbon nanotubes, ranging from experimental synthesis to atomistic and continuum modeling with focus on a variety of properties, behaviors, and applications. The superior mechanical properties of carbon nanotubes are appealing for their potential use in novel nanomaterials. For instance, the Young’s modulus of a single-walled nanotube approaches a terapascal (10^{12} Pa) (Treacy et al., 1996), implying that CNT is one of the strongest known synthesized materials in terms of elastic modulus and ultimate tensile strength (Li et al., 2000b). For over a decade, attempts have been made to utilize the high strength of individual CNTs in an efficient manner. However, a well-known behavior of CNTs is inter-tube bonding due to weak van der Waals interactions, which results in formation of bundles that

* Corresponding author at: Laboratory for Atomistic and Molecular Mechanics, Department of Civil and Environmental Engineering, Massachusetts Institute of Technology, 77 Massachusetts Ave. Room 1-235A&B, Cambridge, MA, USA. Tel.: +1 617 452 2750; fax: +1 617 324 4014.

E-mail address: mbuehler@MIT.EDU (M.J. Buehler).

URL: <http://web.mit.edu/mbuehler/www/>. (M.J. Buehler).

contain hundreds or thousands of individual nanotubes. The formation of these larger-scale structural features complicates investigations of the mechanical properties of nanotube materials, and challenges remain in understanding how to control and measure the properties of such large systems of CNTs. The study of the structural properties of larger-scale bundles of CNTs attached to a surface is the focus of this paper.

1.1. Formation of bundles in nanotube arrays

The interaction of individual CNTs in larger-scale structures often plays a critical role in the mechanical properties of CNT systems. At the nanoscale, weak van der Waals interactions govern the structural organization and the mechanical properties of CNT based materials. For example, the high axial strength of individual nanotubes is lost when nanotubes form bundles as the weak forces allow slippage of nanotubes within a bundle (Ajayan and Banhart, 2002; Kis et al., 2004). Such effects are also found in nanotube based fibers or ropes (Dalton et al., 2003; Zhu et al., 2002), as well as in vertically aligned nanotube arrays (Li et al., 2000a; Liu et al., 2008; Zhang et al., 2008). The importance of the interplay between adhesive forces and covalent bonding at the atomistic, molecular, and global material scales remains poorly understood for many CNT systems. Advancing our understanding of the structural arrangements and mechanisms resulting from such weak interactions is necessary for the development of materials and structures that take advantage of bundling of nanotubes, for example in self-organized CNT based surface materials. Fig. 1 shows snapshots of bundled polymer nanotube structures (Linares et al., 2009; Steinhart et al., 2002), illustrating the type of features and scales associated with bundle formation typically observed in nanotube systems, involving a very large number of nanotubes and structural features at tens and hundreds of nanometers. Modeling these systems requires time- and length-scales beyond the reach of conventional molecular dynamics, and the use of multi-scale approaches is critical to build simulation models of these structures.

The molecular level interactions of adjacent carbon nanotubes has been investigated using atomistic methods (Chen et al., 2003; Liew et al., 2005, 2006; Zhou et al., 2007; Zhu et al., 2004), but bundle formation and self-organization of a large number of CNTs becomes computationally expensive at the atomistic level for relatively long carbon nanotubes, or multiple nanotubes (the computational cost is proportional to the number of atoms in the simulation). Mesoscopic “bead-spring” methods have been proven a viable approach to simulate arrays of CNTs (Buehler, 2006; Cranford and Buehler, 2009) and graphene (Cranford et al., 2009), but these approaches are still limited to hundreds or thousands of nanotubes in a particular nanotube array. Synthesized samples of carbon nanotube arrays have shown bundles consisting of hundreds of thousands of individual CNTs (Bronikowski, 2006). Thus a new approach is required to investigate bundle formation of such large arrays of CNTs. The focal point of this paper is the multi-scale development of a single degree of freedom “lollipop” model for nanotube representation to enable the simulation of structural organization of very large bundles of CNTs. The development of this model is facilitated by a continuum elasticity model used to quantify the energy balance of adhered adjacent carbon nanotubes, where all parameters are identified by full atomistic simulation results. This simulation model has a twofold purpose: first, to confirm bundle formation of synthesized samples at a relatively large scale, and; second, to efficiently investigate the capacity to manipulate bundle formation within large nanotube arrays by introducing geometric changes to the geometry of constituting elements (e.g. patterning). Specifically, parametric investigations concerning nanotube length, spacing, diameters, and other structural and physical parameters can quickly be implemented to manipulate possible bundle formations and attain unique surface and mechanical properties of nanotube arrays. This approach can be used to engineer novel surface nanostructures.

1.2. Outline

The outline for the rest of this paper is as follows. In Section 2 the continuum theory governing nanomechanical bundle formation and equilibrium is described via an energy balance between bending strain energy, local deformation contact

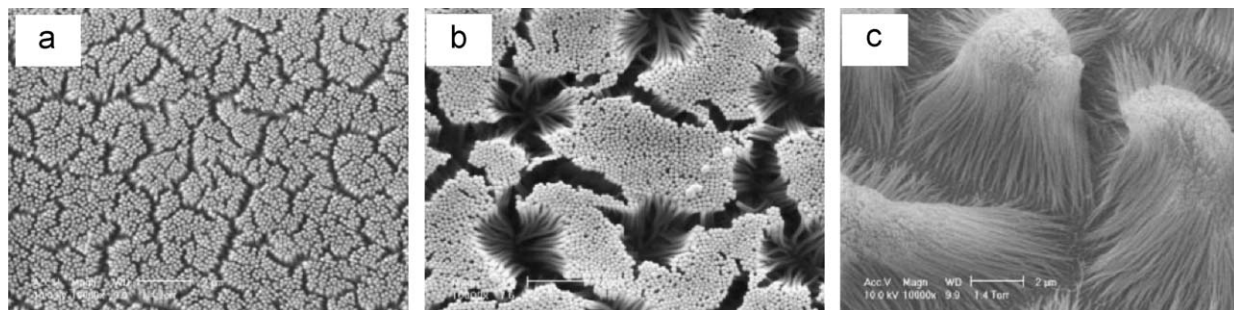


Fig. 1. Illustration of bundle formation in nanotube systems. The images show scanning electron microscopy (SEM) characterization of polymer nanofilament bundles (Linares et al., 2009). Image reprinted with permission from: Linares et al., 2009. Polymer films composed of surface-bound nanofilaments with high aspect ratios, molecularly imprinted with small molecules and proteins. *Advanced Functional Materials* 19, 1299–1303. Copyright Wiley-VCH Verlag GmbH & Co. KGaA. Reproduced with permission.

energy, and adhesion energy. Section 3 describes the fine-trains-coarse multi-scale approach from full atomistic simulations, beginning with a description of the implemented atomistic test suite in Section 3.1. Section 3.2 discusses the limiting equations through the use of mesoscopic nanotube models, and Section 3.3 includes the development of a single degree of freedom (SDOF) model for two types of carbon nanotubes (single-walled and double-walled). Then, in Section 3.4, the simulation methodology implemented with the SDOF model is introduced. In Section 4 we report three examples of large-scale simulations of CNT arrays. The results and implications of the modeling results are discussed in Section 5.

2. Theoretical nanomechanics model

Carbon nanotubes attract each other via van der Waals forces, but in an array of vertically aligned carbon nanotubes, each tube acts as a vertical cantilever. Thus, a balance of bending strain energy, local deformation energy, and adhesion energy effectively limits bundle formation and size. To facilitate the development of limiting equations, nanotube deformation is assumed to occur in two dimensions. For a cylindrical nanotube, the bending strain energy is equal in all directions, and only dependent on the absolute displacement of the cantilevered tip. Further, the attraction force due to van der Waals interactions is non-directional. Finally, the interactions between adjacent nanotubes in MD simulations are eventually governed by pair potentials that are evaluated between two nanotubes at a time, essentially resolving the interactions on a 2D plane. Thus a two dimensional formulation is considered adequate for the theoretical derivation, noting that the MD simulations to be presented are fully 3D.

We assume that all nanotubes are geometrically identical with outer diameter d , wall thickness t , length L , and equally spaced, Δ . We can thus determine the energy changes due to the formation of such a bundle with an arbitrary number of nanotubes (see Fig. 2).

The change of the free energy due to the formation of a bundle consisting of n nanotubes is given by

$$W = \sum_{i=1}^n U_i^b + \sum_{i=1}^n U_i^c - \Delta\gamma \times 2b \sum_{i=1}^n (L-l_i), \quad (1)$$

where $\Delta\gamma$ is the work of adhesion, U_i^b the bending strain energy, U_i^c the strain energy due to local deformation, and l_i the length of non-contact region. As such, it is the formulation and tacit balance of these energies that govern the natural formation of stable bundles in nanotube arrays. A brief derivation of each follows.

2.1. Bending strain energy

Under small deformation, it is assumed that a nanotube behaves as an elastic beam. Neglecting shear deformation, we apply a cantilever model with zero end-rotation via elastic beam theory (Timoshenko and Maccullough, 1940), then

$$U_i^b = \frac{6EI\Delta_i^2}{l_i^3}, \quad (2)$$

where EI is the bending stiffness of the cantilever, Δ_i being the bending deflection, and l_i representing the non-contact or bent length for the i th nanotube. Using the equivalent energy approach assuming beam behavior holds for carbon

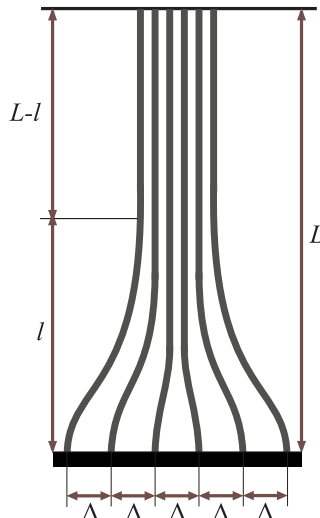


Fig. 2. 2D bundle representation for governing equations in the continuum nanomechanics model where L is total length, l bent length, and Δ inter-tube spacing.

nanotubes has been used in previous investigations for both localized mechanics (Buehler, 2006) and array behavior (Qi et al., 2003).

2.2. Local deformation energy stored in the contact region

In general, the adhesive contact between two tubes will cause local deformation around the contact region, in which strain energy is stored as well. For two identical circular cylinders subject to no external load, this part of energy is given by Glassmaker et al. (2004)

$$U_i^c = (L-l_i) \left(\frac{b}{2} \right) \Delta\gamma, \quad (3)$$

where $(L-l_i)$ represents the contact length, $\Delta\gamma$ is the work of adhesion, and b stands for the half-width of the contact area, as shown in Fig. 3(a). However, for the case of the carbon nanotubes considered here (that is, tubes with relatively small diameter), the equilibrium spacing due to van der Waals interactions is such that there is minimal contact deformation. The equilibrium distance between the axial centers of adjacent nanotubes is greater than the diameter—one of the contributing factors to the slippage observed in nanotube bundles. Local deformations are more prevalent with nanotube–substrate interactions. In such a case, the deformation energy may govern and require contact area calculations. Such a contribution is included in the current discussion for completeness. Albeit, for the current model it can be demonstrated that the local deformation due to the inter-tube interactions is relatively small. We therefore neglect it by taking $b=0$ (see Fig. 3(b)) and $U_i^c \approx 0$ as previous studies did (Chen et al., 2003; Zhou et al., 2007). This assumption consequently turns the work of adhesion per contact surface area, $\Delta\gamma$, into adhesion energy per contact length, E_L (see Section 2.3).

2.3. Adhesion energy

The adhesion energy is a direct consequence of van de Waals interactions and atomic attraction between adjacent nanotubes. The adhesion energy can be used in either energy per unit area ($\Delta\gamma$) when the contact surface is to be considered, or energy per unit length, E_L , when there is no contact in equilibrium.

For contact (Fig. 3(a)) we let

$$W_{adhesion} = -\Delta\gamma \times 2b \sum_{i=1}^n (L-l_i), \quad (4a)$$

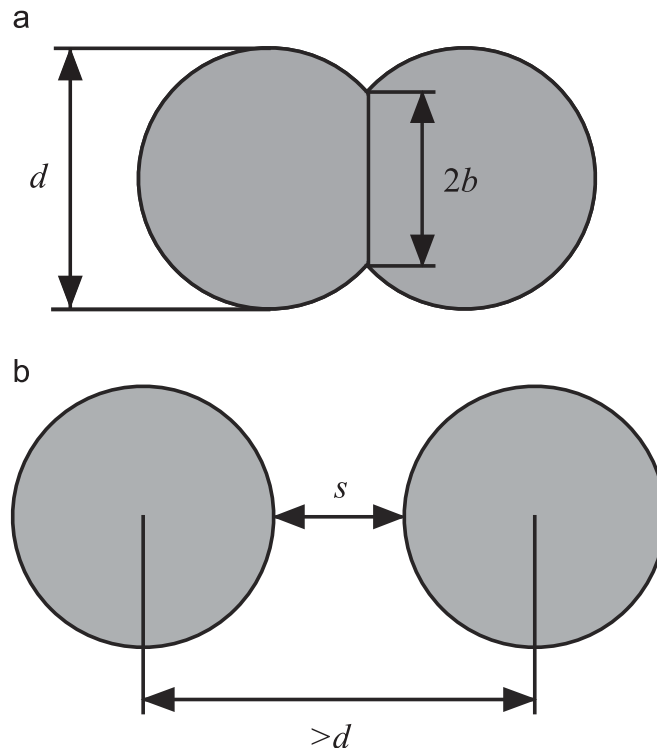


Fig. 3. Contact and non-contact cases for surface deformation energy: (a) contact with local deformation and (b) non contact equilibrium.

again where $(L-l_i)$ represents the contact length, $\Delta\gamma$ the work of adhesion, and b stands for the half-width of the contact area. For non-contact (Fig. 3(b)) we let

$$W_{adhesion} = -E_L \sum_{i=1}^n (L-l_i), \quad (4b)$$

where E_L represents the adhesion (or interaction) energy per unit length of nanotube, whose value is determined via atomistic simulations.

2.4. Equilibrium condition

With minimal local deformation, or $U_i^c \approx 0$, and using adhesion energy per unit length, E_L , then the above general free energy expression (Eq. (1)) is simplified to

$$W = \sum_{pairs} U_i^b - \sum_{pairs} E_L(L-l_i), \quad (5a)$$

or, for each nanotube pair

$$W_i = U_i^b - E_L(L-l_i) = \frac{6EI\Delta_i^2}{l_i^3} - E_L(L-l_i). \quad (5b)$$

For any two nanotubes in equilibrium contact, we have

$$\frac{\partial W_i}{\partial l_i} = \frac{\partial}{\partial l_i} \left(\frac{6EI\Delta_i^2}{l_i^3} - E_L(L-l_i) \right) = 0, \quad (6)$$

which gives rise to the relation between adhesion energy (E_L), nanotube stiffness (EI), nanotube spacing (Δ_i), and required bent length (l_i) of a given nanotubes (note that the nanotube spacing is equal to the required deflection [or bending displacement] for adhesion)

$$l_i = \left[\frac{18EI\Delta_i^2}{E_L} \right]^{1/4} \leq L. \quad (7)$$

Note that the bent length (or non-contact length) at equilibrium is a function of a single variable, the bending displacement, Δ_i , in addition to two constants (with respect to nanotube type): (1) adhesion energy per unit length, E_L , and (2) bending stiffness, EI . A similar result was developed for the stability of adhered punching plates for microcontact printing (Hui et al., 2002).

3. Fine-trains-coarse multi-scale approach

We implement a “fine-trains-coarse” approach to develop a single degree of freedom (SDOF) model derived solely from atomistic calculations. A series of full atomistic calculations of mechanical test cases (test suite) is applied via classical molecular dynamics to derive a simplified set of parameters to describe the nanotube behavior at a coarser level.

3.1. Full atomistic simulations

The test suite implemented to determine the parameters required for the coarse-grain SDOF nanotube consists of the following three cases: (i) tensile loading to determine Young’s modulus, E ; (ii) bending to determine the bending stiffness, EI , and; (iii) an assembly of two nanotubes to determine the adhesion energy, E_L (the adhesion energy per unit length of any two nanotubes, or any two macromolecules is presumed constant, based on the fundamental physical interaction between atoms or molecules). The test suite is applied using two types of carbon nanotubes: (i) a (5,5) armchair single walled carbon nanotube and (ii) a multi-walled carbon nanotube consisting of an inner (8,8) armchair CNT with an outer (12,12) armchair CNT (a double walled carbon nanotube), as depicted in Fig. 4(a) and (b), respectively. We use a Tersoff potential to describe the carbon bonding within tubes, and a Lennard–Jones potential to describe inter-tube interactions. A more detailed description of the atomistic simulations and results for SWCNTs can be found in Ref. Buehler (2006). The same procedure is applied here to DWCNTs. Here, we provide only a brief review of the multi-scale approach.

A tensile test is applied to each nanotube conformation by fixing one end and applying displacement to the opposite end at varying speeds. The resulting force–displacement relationship is converted to a stress–strain relationship by assuming the force is applied to a circular cross-section of the nanotube (a similar approach used in Buehler (2006)). Considering small deformation only, Young’s modulus is calculated by

$$E = \frac{\partial \sigma}{\partial \epsilon} \approx \frac{\Delta \sigma}{\Delta \epsilon}. \quad (8)$$

Similarly, a bending test is implemented by fixing one end of the nanotube and applying a lateral force to the opposite end, effectively cantilever bending. Through elastic beam theory, the bending stiffness is calculated as

$$EI = \frac{FL^3}{3\Delta}. \quad (9)$$

For adhesion simulations, two nanotubes are simulated together, moved into close proximity to one another, and then separated, with an energy minimization procedure undertaken at discrete distances. The equilibrium spacing is taken as the position of minimum potential energy, while the adhesion energy is calculated via differences in potential at equilibrium and at separation. Table 1 summarizes the results of all atomistic simulations.

3.2. Mesoscale bead–spring model

The single degree of freedom model is developed directly from the atomistic simulations, without the need for the development of a mesoscale, bead–spring model. However, to substantiate the parameters determined by full atomistic simulations, the bead–spring model is a useful tool to confirm the governing equations described in Section 2. Further, a bead–spring model allows the degrees of freedom necessary to correlate the non-contact lengths of bundled nanotubes as described by Eq. (7). Only a brief description of the formulation of the bead–spring model is given for brevity. For a more detailed description and application see Buehler (2006); Cranford and Buehler (2009). The basis of the mesoscale model is represented by a function of the total energy of the system expressed as

$$\phi_{\text{System}} = \phi_T + \phi_B + \phi_{\text{weak}}, \quad (10)$$

where ϕ_T is the energy stored in the chemical bonds due to axial stretching, ϕ_B the energy due to bending, and ϕ_{weak} the energy due to weak interactions. The total energy contribution of each is calculated by a sum over all pair-wise (distance) and triple (angular) interactions in the system. For axial stretching a simple harmonic spring is used to determine the energy between all pairs of particles in the system, given by

$$\phi_T(r) = \frac{1}{2}k_T(r-r_0)^2, \quad (11)$$

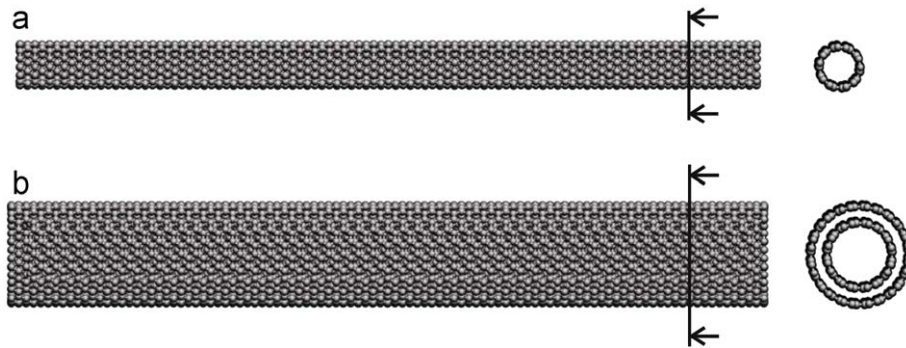


Fig. 4. Full atomistic models of: (a) (5,5) armchair single-walled carbon nanotube and (b) (8,8) inner, (12,12) outer double-walled carbon nanotube.

Table 1

Summary of results from full atomistic simulations (for specific CNT geometries).

Parameter	Value	Units
1. SWCNT		
Young's modulus, E	2.0×10^{12}	N/m ²
Bending stiffness, EI	6.65×10^{-26}	Nm ²
2. DWCNT		
Young's modulus, E	1.3×10^{12}	N/m ²
Bending stiffness, EI	8.30×10^{-25}	Nm ²
3. Adhesion energy and equilibrium spacing ^a		
SWCNT (5,5)	2.31×10^{-10}	J/m
	13.1	Å
DWCNT (8,8)–(12,12)	3.30×10^{-10}	J/m
	22.1	Å

^a The defined adhesion energy is per unit length. The equilibrium spacing is defined here as the center-to-center spacing of the nanotubes at equilibrium, not the spacing between adjacent nanotube walls. The adhesion energy for larger tubes may be affected by additional effects s.a. CNT flattening that may further increase the adhesion energy. These effects are not considered here and the results are only valid for the specific CNT geometries under investigation.

Table 2
Summary of bead–spring parameters for mesoscale model^a.

Parameter	SWCNT (5,5)	DWCNT (8,8)-(12,12)
k_T	1000 kcal/mol/Å ²	1880 kcal/mol/Å ²
r_0	10 Å	20 Å
k_B	14,300 kcal/mol/rad ²	90,000 kcal/mol/rad ²
φ_0	180°	180°
$\sigma_{LJ,*}$	9.35 Å	19.7 Å
$\varepsilon_{LJ,*}$	15.1 kcal/mol	43.2 kcal/mol

^a The adhesion parameters in the mesoscale model depend on the size and structure of the tubes considered. The parameters reported here are only valid for the specific CNT geometries modeled here.

with k_T as the spring constant relating distance, r , between two particles. For bending, the bending energy is given by a sum over all triples in the system, given by

$$\phi_B(\varphi) = \frac{1}{2} k_B (\varphi - \varphi_0)^2, \quad (12)$$

with k_B as the spring constant relating bending angle, φ , between three particles. Weak interactions (vdW) are defined by a Leonard–Jones 12:6 function, given by

$$\phi_{weak}(r) = 4\varepsilon_{LJ,*} \left(\left[\frac{\sigma_{LJ,*}}{r} \right]^{12} - \left[\frac{\sigma_{LJ,*}}{r} \right]^6 \right), \quad (13)$$

where r is the atomic separation, $\varepsilon_{LJ,*}$ represents the energy minimum at equilibrium and $\sigma_{LJ,*}$ as the distance parameter.

Thus, the mesoscopic model is defined by six parameters: k_T ; r_0 ; k_B ; φ_0 ; $\sigma_{LJ,*}$; and $\varepsilon_{LJ,*}$. The results from the above atomistic simulations are used to determine the six parameters via equilibrium conditions (r_0 ; φ_0 ; $\sigma_{LJ,*}$) and energy conservation (k_T ; k_B ; $\varepsilon_{LJ,*}$). For a more detailed description of the parameter derivations, the reader is referred to Buehler (2006). All parameters are defined solely from the atomistic results given in Table 1, and given in Table 2. It is noted that the formulation using simple harmonic potentials is suitable for small deformations only. However, for investigations concerning bundle formation, the small deformation assumption is valid.

The simulations are carried out using the massively parallelized modeling code LAMMPS (Plimpton, 1995)¹ capable of running on large computing clusters. The mesoscale investigations reported were carried out on single CPU Linux workstations.

3.2.1. Mesoscale simulations and limiting equations

We perform a series of simulations to test the validity of Eq. (7), and illustrate the bundling behavior of carbon nanotubes. Relatively small-scale simulations of nanotube arrays consisting of hundreds of bead–spring elements are implemented to investigate the parameters of Eq. (7) (see Fig. 5 for an illustrative array). The simulations are focused on: (1) the independence of bent length with respect to total length of the nanotube; (2) the correlation between required bending displacement (i.e. adjacent nanotube spacing), and adhered length; (3) the effective difference in bending stiffness and adhesion strength (i.e. SWCNT compared to DWCNT).

To confirm the bent length is independent of total length, two simulations of pairs of (5,5) SWCNTs are presented. The first pair is 50 nm in length, while the second pair is 100 nm in length. Both pairs are spaced 5 nm, requiring a bending displacement of $\Delta=2.5$ nm. Via Eq. (7), the bent length is calculated to be approximately 134 Å. Simulated results depict a bent length of 141 and 151 Å for the first and second pair, respectively (Fig. 6(a)). The bead–spring model is considered in “contact” when adjacent beads are within the equilibrium distance (9.35 Å for SWCNT) $\pm 10\%$ to account for dynamic fluctuations in the simulation. The slight deviation from the calculated value is attributed to the asymmetry in the bending of the nanotubes. If the bending displacement of one is increased (e.g. $\Delta > 2.5$ nm), the nanotube requires an increased bent length. It is noted that by Eq. (7), $l \propto \sqrt{\Delta}$, so a slight deviation in Δ resulting from the random dynamics of the simulation results in discrepancy in bent lengths from theoretical values.

To confirm the relation with required displacement, nanotube spacing is varied from 3 to 5 nm. The results of pairs of (5,5) SWCNT with equal height (50 nm) are shown in Fig. 6(b). Calculated bent lengths are 104 Å for 3 nm spacing and 134 Å for 5 nm spacing, compared to the simulation results of 115 and 141 Å, respectively. As before, slight deviations from the calculated value is attributed to asymmetric bending of nanotube pairs.

Finally, a pair of DWCNTs is compared to the equivalent geometry of SWCNTs (both 50 nm in height, 5 nm spacing). As shown in Fig. 6(c) the increase in stiffness of a DWCNT greatly increases the required bent length both calculated (231 Å for DWCNT compared to 134 Å for SWCNT) and simulations (230 and 141 Å, respectively).

¹ See: <http://lammms.sandia.gov/>.

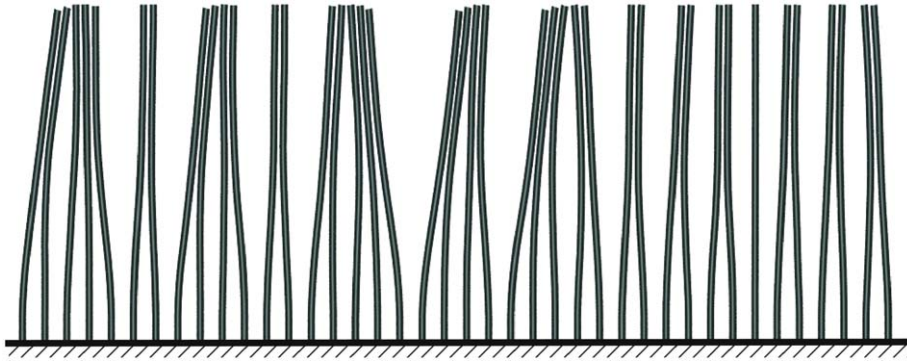


Fig. 5. Mesoscale bead-spring nanotube simulation, 40 DWCNTs (height of 50 nm, spacing of 5 nm), illustrating the propensity of nanotubes to form bundles via van der Waals interactions.

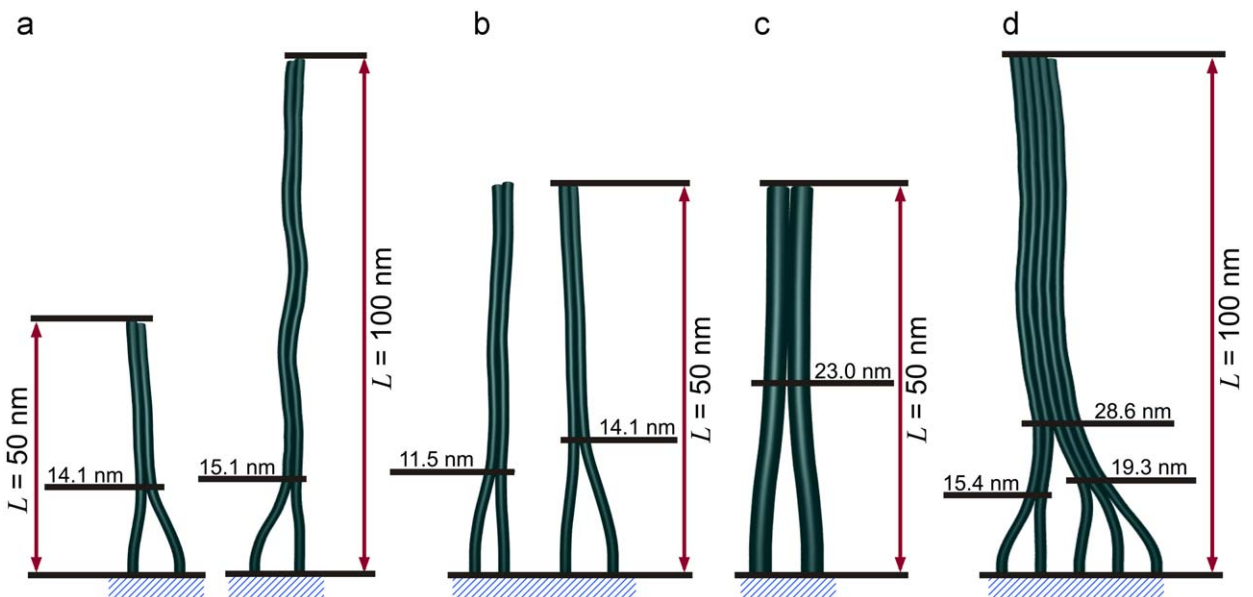


Fig. 6. Meso-scale simulation confirmation of the theoretical nanomechanical model: (a) variable length (5,5) SWCNT pairs (50 and 100 nm); (b) variable spaced (5,5) SWCNT pairs (50 nm height with 3 and 5 nm spacing); (c) DWCNTs with 50 nm height and 5 nm spacing; bent length of 230 Å; (d) hierarchical bundle formation; SWCNTs with 100 nm height and 5 nm spacing. The dashed lines and numbers are predictions from the theoretical nanomechanical model. The agreement between the simulation results and the model can be seen in the images.

When multiple nanotubes are simulated, the increase in displacement for the outer nanotubes towards the “bundle center” requires an increase in bent length (as anticipated). However, the same tubes are in contact with adjacent nanotubes with approximately the calculated bent lengths (see Fig. 6(d)). This creates a hierarchy of smaller bundles aggregating in larger bundles. Irrespective, the final bent (or contact) length between any pair of nanotubes is well described by the derived governing equation. It is also noted that the formed bundles are stable under relatively long simulations (approaching a scale of micro-seconds). We further note that a large cutoff of 200 Å (with interactions between all particles) was used in the simulations.

The results from these relatively small simulations depict accurate prediction of non-contact lengths. Thus, validated by simple mesoscale bead-spring simulations, the relation described by Eq. (7) is used as the basis for formulation and behavior of a single degree of freedom (SDOF) lollipop model.

3.3. SDOF “lollipop” model

Unlike the mesoscopic bead-spring model, the SDOF model need only represent the behavior of a carbon nanotube at the global level—i.e. total elastic deformation (deflection) and inter-tube adhesion. It is again stressed that the SDOF model is not derived from the bead-spring model, but rather from the full atomistic simulations, essentially reducing the mechanical properties of a carbon nanotube to a set of equations describing the motion and interaction of single masses

(Fig. 7). Similarly, the SDOF model is represented by a function of the total energy of the system expressed in Eq. (11), or

$$\phi_{\text{System}} = \phi_T + \phi_B + \phi_{\text{weak}}. \quad (14)$$

However, unlike the mesoscopic bead–spring model, which develops potentials for the nanotube in a piece-wise manner, the formulation of each term of the SDOF model considers the entire nanotube. The model itself consists of three particles, which are required to calculate relative angles. However, two of the particles are fixed, massless “dummy” particles (Fig. 7), which do not affect the simulation process.

3.3.1. Pair potential and structural rigidity

For axial behavior a simple harmonic potential is implemented, where

$$\phi_T(L) = \frac{1}{2} K_T (L - L_0)^2. \quad (15)$$

As seen, the potential is formulated in terms of total length of the nanotube (rather than equilibrium spacing of the beads/spring), with L_0 equaling the unloaded, relaxed length of the tube, and L representing current tube length. Again, small deformation is assumed, as bundle formation will not impose large axial strains.

3.3.2. Rotational and bending stiffnesses

Rather than a simple harmonic potential to represent bending energy, the potential is formulated through beam theory for a fixed–fixed cantilevered beam (Fig. 8(a)). The length of the beam is taken as the *bent length* of each nanotube (l_i). The applied moment at the fixed ends is thus

$$M = \frac{6EI\Delta}{l_i^2}, \quad (16)$$

while the equivalent force is taken as

$$F = \frac{M}{l_i}. \quad (17)$$

It can be easily shown that the bending energy from this formulation is the same bending energy as shown in Eq. (2). We then related the force to the total angle due to the bending displacement. From Fig. 8(b)

$$\frac{\Delta}{L} = \tan \theta = \frac{1}{L} \frac{F l_i^3}{6EI}, \quad (18a)$$

where L is the total length of the nanotube. Leading to

$$F = \left[\frac{6EIL}{l_i^3} \right] \tan \theta, \quad (18b)$$

$$F = \left[\frac{6K_b L}{l_i^3} \right] \tan(\varphi - \varphi_0), \quad (18c)$$

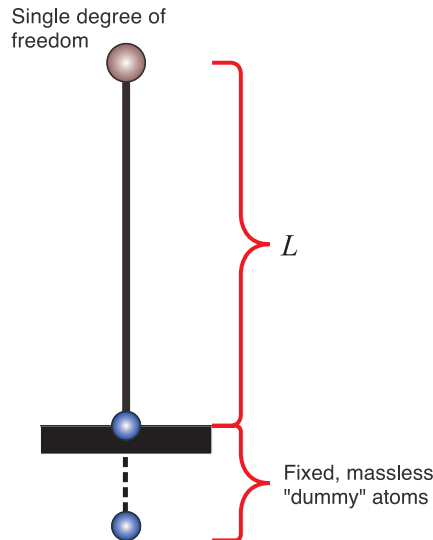


Fig. 7. Single degree of freedom “lollipop” model of CNTs. An entire CNT of length L is represented by a single particle.

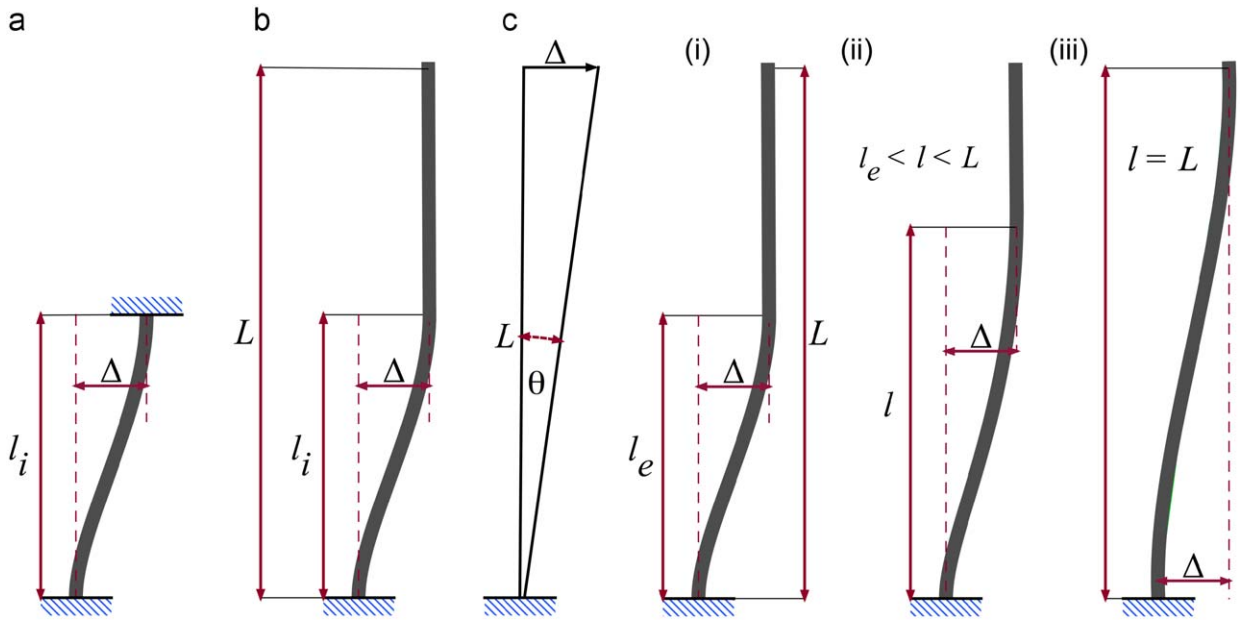


Fig. 8. Beam theory assumptions: (a) fixed–fixed beam under displacement; (b) bending angle approximation; (c) changing of bent length, l , with bundle conformation: (i) nanotube in bundled conformation, equilibrium bent length, $l=l_e$; (ii) intermediate conformation, bent length $l_e < l < L$; (iii) final adhered conformation, bent length equal to total length, $l=L$.

where l_i is the required bent length calculated from Eq. (7), L the total length of the nanotube, K_b the bending stiffness of the entire nanotube (theoretically equivalent to EI ; used to distinguish from traditional elastic bending stiffness), φ the angle of the nanotube, and φ_0 the equilibrium angle ($\varphi_0=180^\circ$).

The above bending force (or resistance to bending) relation is only for specific fixed–fixed conformations of the nanotube. Before bundling, the nanotube is free to bend in any arbitrary manner. What is known is only the end conformation, when the nanotubes are bundled. As the resistance to bending and bending stiffness is a limiting parameter for bundle formation, and knowledge of the tubes propensity to bundle can be used to formulate suitable force–bending relationship. As the bending resistance is inversely proportional to the bent length, it follows that the force approaches a minimum as the bent length approaches the total length of the tube. Due to the adhesion of nanotubes, when adjacent nanotubes are separated, the bent length can be considered to approach the total length, as depicted in Fig. 8(c).

It is an assumption of the model that this force ultimately determines if two adjacent nanotubes remain adhered. Implementing this assumption *a priori* as the force required to effectively “unbundled” two adhered nanotubes, then

$$F_{min} = \left[\frac{6K_b}{L^2} \right] \tan(\varphi - \varphi_0). \quad (19)$$

Thus, instead of two parameters to define the bending potential (k_b and φ_0) as in the bead–spring model, three are required for the SDOF model: K_b , φ_0 , and L . An increase in length of the nanotube changes resistance to bending, reducing the bending stiffness of the entire nanotube. The bent (or non-contact) length, l_i , however, is only explicitly defined at equilibrium, and is free to vary while the nanotube is in intermediate, non-bundled states.

3.3.3. Adhesion interactions

A common representation of van der Waals interactions between carbon nanotubes is obtained again via the Lennard–Jones 12:6 potential (see Eq. (13)).

For bundled tubes, the energy minimized energy between two tubes in equilibrium changes as a function of the bent length and contact region. The model assumes that the interaction between the non-contact regions of the nanotubes is negligible. For carbon, van der Waals force becomes negligible once the atom exceeds a distance on the order of one nanometer (Brenner et al., 1993). Using the deflection profile from the assumed elastic beam model, the increase in interaction energy was calculated numerically for nanotube spacing (center-to-center) from 1.0 to 4.0 nm, using the bending stiffness and adhesion energy parameters for (5,5) SWCNT at a length of 50 nm. The maximum increase in potential energy was approximately 7% when the nanotubes were within close proximity to each other (a relatively shallow bending profile). The increase dropped to less than 3% when the nanotubes were spaced over 2 nm. Such a minimal increase does not significantly change the total interaction energy, and thus considering the contact region only is deemed adequate, an assumption also presumed by previous studies (Chen et al., 2003).

Considering the contact region at equilibrium distance, the equilibrium energy is expressed as

$$\varepsilon_{ij}^* = \frac{1}{2} E_L L, \quad (20)$$

$$\varepsilon_{ij} = \mu \times \varepsilon_{ij}^*, \quad (21)$$

where μ is a scaling parameter defined by the contact length

$$\mu = \frac{L - l_i}{L}, \quad (22)$$

where L is the total length of the nanotube, E_L the adhesion energy per unit length, and l_i is the bent length for each tube as calculated by Eq. (7). This results in a modified Lennard–Jones potential

$$\phi_{weak}(r_{ij}) = 4\mu\varepsilon_{ij}^* \left(\left[\frac{\sigma_{ij}}{r_{ij}} \right]^{12} - \left[\frac{\sigma_{ij}}{r_{ij}} \right]^6 \right), \quad (23)$$

where r and σ_{ij} are defined as before, μ determined by Eq. (22), and ε_{ij}^* from Eq. (20).

3.4. Computational approach

The SDOF model is implemented using a modified version of the modeling code LAMMPS (Plimpton, 1995). The LAMMPS code was extended to enable the treatment of the nanotube interactions discussed in Section 3.3, specifically the functions for angle and pair potentials, which significantly differ from traditional molecular dynamic implementations. The angle function was modified according to Eq. (19), while the pair potential implements an on-the-fly modification of the energy parameter, ε_{ij} , of the Lennard–Jones potential via Eq. (23) according to the required bending length of Eq. (7).

Arrays are generated with specified regular spacing, nanotube height, and nanotube type (SWCNT or DWCNT). An NVT ensemble (Hoover, 1985) is implemented with a temperature of 300 K. Arrays are simulated with a time step of 10 fs, with a total time of 5.0 ns. Although a relatively short molecular simulation, longer runs are not required for the current investigation as the goal is merely attaining equilibrium. As some parameters are a function of the length of the nanotube model, Table 3 presents the parameters for nanotubes 1000 nm in length. It is noted that the tubes are simulated in a vacuum, thereby neglecting any effects from the surface or array substrate.

3.5. Comparison between bead–spring and SDOF “lollipop” models

Both the mesoscopic bead–spring model and the SDOF “lollipop” models are developed under the assertion of energy conservation between full atomistic and equivalent coarse-grain potential behavior via explicit potentials for axial stretching, bending, and intra-molecular interactions (e.g. Eq. (10) and Eq. (14), respectively). The approach for each differs in the implementation of the coarse-grain parameters. For the bead–spring model, each potential describes *local* behavior (on the order of 10 to 20 Å), and the mesoscale model is segmented into multiple bead–spring elements. Such a representation has the advantage of modeling the deformation of a nanotube under a number of loading conditions. However, the number of degrees of freedom is scaled with the length of the nanotube, and becomes computationally expensive when either large arrays (e.g. thousands of nanotubes) or long nanotubes (approaching micrometers) are considered. The SDOF “lollipop” model attempts to circumvent this limitation by asserting energy conservation to the *global* behavior of the nanotube. With each nanotube represented by a single moving particle the degrees of freedom to simulate scales with the number of nanotubes rather than physical represented dimensions (i.e. there is the same number of degrees of freedom for nanotubes of 100 Å or 100 μm in length).

Table 3

Summary of parameters for a 1000 nm SDOF “lollipop” model^a.

Parameter	SWCNT (5,5)	DWCNT (8,8)-(12,12)
k_T	1,000,000 kcal/mol/Å ²	1,880,000 kcal/mol/Å ²
r_0	10,000 Å	10,000 Å
k_B	95,800 kcal/mol Å	1,195,600 kcal/mol Å
φ_0	180°	180°
L	10,000 Å	10,000 Å
σ_{ij}	9.35 Å	19.7 Å
ε_{ij}^*	16,625 kcal/mol	23,750 kcal/mol
E_L	2.31×10^{-10} J/m	3.30×10^{-10} J/m

Note: E_L is required for Eq. (7).

^a The adhesion parameters in the “lollipop” model depend on the size and geometry of the tubes considered. The parameters reported here are only valid for the specific CNT geometries modeled here.

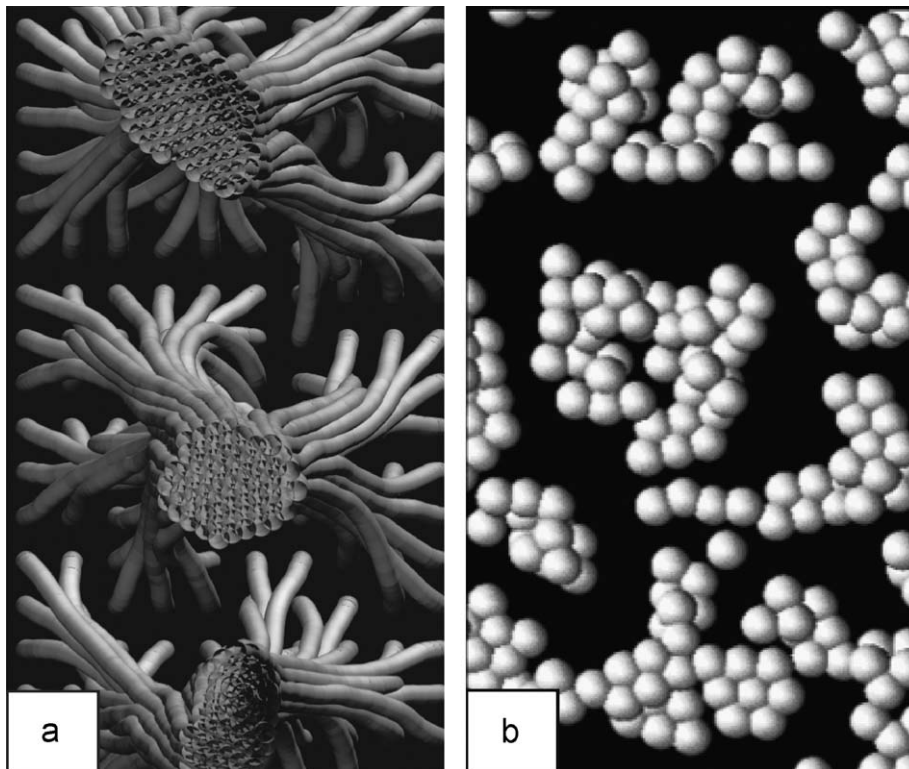


Fig. 9. Comparison of bundle formation characteristics, obtained using the bead–spring model and the SDOF model. The images show top views of nanotubes of 100 nm length and 3 nm spacing. (a) Bead–spring mesoscale model, resulting in an average cluster diameter of approximately 80 Å. (b) SDOF “lollipop” representation, with an average cluster diameter of approximately 70 Å. The SDOF “lollipop” model results in clusters of approximately the same size as the bead–spring representation, validating the approach.

The SDOF “lollipop” model lacks any description of local behavior of the nanotube as compared to full atomistic or bead–spring models. The application of a SDOF representation is practical when local behavior is known *a priori*, and the focus of investigation is on a global, intra-molecular scale. This occurs for carbon nanotube bundling, when the deformed shape of the nanotube is of little concern and the interest is specifically in modeling the overall larger-scale structural organization of the nanotube system.

Comparing a simple simulation of nanotubes, 100 nm in length and spaced 3 nm (Fig. 9), with both a mesoscopic bead–spring and SDOF “lollipop” representation illustrates the critical difference; while the bead–spring representation depicts an accurate deformed shape of the carbon nanotubes, both simulations resulted in similar bundle formation (or adhered nanotubes). The deformation and intra-molecular interactions of the SDOF model is implicit in its development. The diameters of the clusters are taken directly from the simulation results for comparison. The bead–spring representation results in an average cluster diameter of approximately 80 Å while the SDOF “lollipop” representation results in an average diameter of 70 Å. The bead–spring simulation results in slightly larger cluster sizes as the freedom of motion of the model allows for more dynamic configurations. It is noted the bead–spring representation required over one hundred times more elements and computational time than the SDOF representation. It is noted that the variation is on the order of one “concentric ring” of nanotubes to the cluster (the nanotubes in question are on the order of 7 Å in diameter). Although the number of tubes within the cluster is larger, the bundle density does not change significantly.

4. Examples and analysis

Simulations are prepared to investigate nanotube arrays of different aspect ratios (defined as the ratio of height to diameter) and the effectiveness of the SDOF model.

4.1. Example 1: large scale, small aspect ratio homogeneous arrays

To illustrate the relative efficiency of a SDOF representation of a nanotube array, a relatively large-scale array consisting of one million (1000×1000) nanotube representations is simulated. Each “lollipop” nanotube model is 100 nm in height,

with an aspect ratio of approximately 150. The spacing is 20 Å in each direction center-to-center, and periodic boundary conditions are implemented. Other initial patterns were simulated, including a regular triangular grid, and a “pseudo”-random grid (20 Å spacing in each direction with a randomly generated offset of 0–5 Å). The slight changes in initial arrangements did not significantly affect the bundling behavior. Only results corresponding to regular spacing is presented here for consistency.

It is noted that in the present study we implemented a uniform, regular array of carbon nanotubes to allow for a direct comparison with the specific parameters we varied (s.a. spacing, aspect ratio, stiffness, etc.). Furthermore, due to the relatively high aspect ratios of the nanotubes, minor deviations from regular spacing will still result in a close-packed hexagonal arrangement at the bundle tips (see Fig. 9, for example). Significant deviations from regular spacing or their radius could be easily implemented to intentionally manipulate such bundles, but the current investigation was focused on model verification. Such investigations could be carried out in future studies that could be focused on a vast amount of other variables and heterogeneous systems, such as geometric grid arrangement, varying height within the same array, random assortment of SWCNTs with DWCNTs, and others.

If full atomistic methods were implemented on such an array, it would consist of approximately 16 billion atoms, associated potentials, and required calculations. Thus, such a large-scale array is beyond the reach of traditional all-atom molecular dynamics, in particular in light of the required time-scales needed to simulate the self-organization of the tubes. The “lollipop” SDOF representation was simulated on a single CPU with a computational time of under 48 h for a simulation time of 5 ns.

As depicted in Fig. 10(b), relatively small aspect ratios do not result in large bundle formation. The interaction between adjacent nanotubes results in irregular spacing and nanotube adhesion, without distinct clusters of nanotubes.

4.2. Example 2: large aspect ratio homogeneous arrays

To investigate the bundling phenomena, arrays of the dimensions depicted in Example 1 are not required. To simulate an array with an increased aspect ratio, an array of 200 × 200 nanotubes with periodic boundary conditions is implemented. Each “lollipop” nanotube model is 1000 nm in height, with an aspect ratio of approximately 1500. Again, the spacing is 20 Å in each direction center-to-center, and periodic boundary conditions are implemented.

Increasing the height of the nanotubes to 1000 nm effectively reduces the resistance to bending (e.g. Eq. (19)). As a result, as the aspect ratio increases, bundles are more distinct and the nanotubes form denser clusters (Fig. 10(d)).

4.3. Comparison through local density distribution

To quantify the effect of increasing the aspect ratio (nanotube height), a radial distribution function (RDF) is calculated for the simulations described in Sections 4.1 and 4.2. It is the intent that a comparison between local density and global trends can discriminate between random and clustered arrangements, and further provide a methodology of evaluating the extent of cluster sizes. Similar local density approaches have previously been implemented in the characterization of clustering in discontinuously reinforced composites (Cetin and Kalkanli, 2009; Scalón et al., 2003). The radial distribution function is a means to account for the molecular distributions arising from the forces particles exert on each other. Traditionally, the radial distribution function is given by

$$g(r) = \frac{\rho(r)}{\rho_0}, \quad (24)$$

where $g(r)$ is simply the ratio of the local particle density at a distance r , $\rho(r)$, to the global density of the particles in the simulation box, ρ_0 . Any deviation of $g(r)$ from the initial distribution reflects correlation between particles due to intermolecular interactions (i.e. nanotube clusters). To compare the two simulations with vastly different simulation box sizes (and thus difference of global densities, ρ_0) the local density is preferred, where

$$\rho(r) = g(r)\rho_0. \quad (25)$$

The radial density is calculated for each particle in the system by considering each particle as the center of expanding volumetric shells. The local density is taken as the average RDF multiplied by the global density of all particles in the simulation. A propensity to cluster will lead to peaks in the local density at equilibrium spacing(s). It is noted that the local density is calculated under a volumetric spherical shells of discrete radii, but the SDOF bundles are essentially planar. A high density at a given radius correlated to a large number of nanotubes clustered about the particle, as shown in Fig. 11.

For the 100 nm nanotubes (Example 1, Section 4.1) there is a single peak in local density at a distance equal to the equilibrium “contact” distance (r_0). This reflects the nanotubes inclination for attraction. Lack of a second peak, and the relatively uniform local density for $r > r_0$ indicates relatively small cluster formation. The results for the 1000 nm nanotubes (Example 2, Section 4.2) reflect a significant increase in local density at the equilibrium distance, approximately five times greater than the shorter, 100 nm nanotubes, correlating to a higher percentage of adhered nanotubes. Further, there is a reduced peak between approximately 1.4–2.1 times the equilibrium distances, followed by a smaller peak at approximately 2.5 the equilibrium distance, indicating adhesion and clustering of next-nearest neighbors (see Fig. 11(a)).

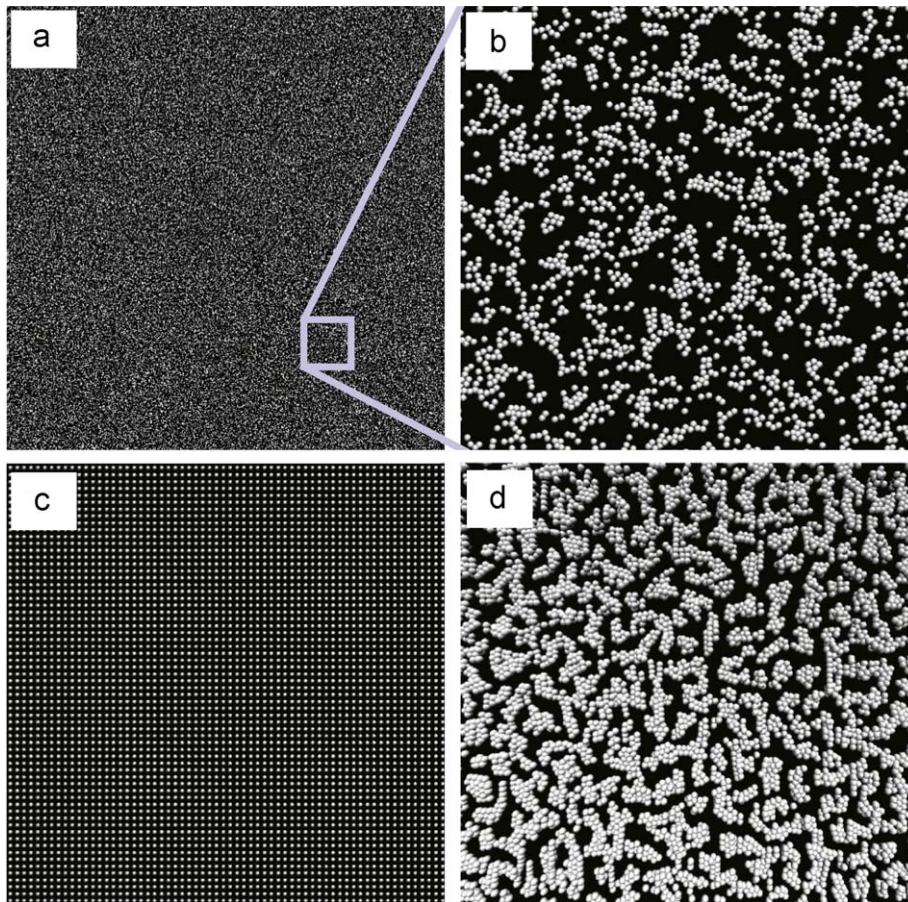


Fig. 10. Large-scale array of SWCNT depicting cluster formation with variable aspect ratios. (a) Aspect ratio=150, dimensions: approx. $1.0 \mu\text{m} \times 1.0 \mu\text{m}$; micrometer array used to illustrate the extent of scale for applications; (b) aspect ratio=150, dimensions: approx. $0.1 \mu\text{m} \times 0.1 \mu\text{m}$; (c) aspect ratio=1500; dimensions: approx. $0.15 \mu\text{m} \times 0.15 \mu\text{m}$, initial configuration depicted for comparison; (d) aspect ratio=1500; dimensions: approx. $0.15 \mu\text{m} \times 0.15 \mu\text{m}$, bundled configuration. Comparison of bundled configurations (b) and (d) indicates an increase in bundle size and density for the higher aspect ratios.

For both simulations, the local density is calculated with a cutoff distance of 40 \AA . For comparison, the initial local density distribution is calculated via the initial configuration (i.e. shown in Fig. 10(c)).

The definition of a nanotube cluster can be subjective with respect to number of included nanotubes, however the presence of clustering can be inferred when the local density about a particular nanotube exceeds a certain threshold value (Cetin and Kalkanli, 2009; Prodanov et al., 2007). Such a threshold can be dependent on the intended application of the nanotube array. A comparison of the local densities via the radial density function is an effective discriminator of cluster size and can successfully be used for quantitative characterization of nanotube clusters.

4.4. Effect of surface energy on relative cluster size

Carbon nanotubes form large and stable clusters due to the weak van der Waals interactions between carbon atoms. It had been shown that the surface energy of carbon nanotubes can be intentionally manipulated in fabrication (Al-Haik et al., 2005) or *in situ* (Rueckes et al., 2000). Similar inter-tube attraction and adhesion also occurs on nanotube arrays (Linares et al., 2009). The surface energy of nanotubes provides the driving force for bundling and cluster formation. As described in Section 2, nanotube bundling is dictated by the competition between strain/deformation energy and the adhesion energy.

To investigate this dependence the surface energy is subsequently varied to show the effect on bundling and cluster size. Equivalent simulations of Example 1 were undertaken, varying the surface energy from 25% to 250% of the actual value of $2.31 \times 10^{-10} \text{ J/m}$ for (5,5) SWCNT. For each value of surface energy, the local density distribution is calculated, and the peak local density determined at the equilibrium spacing, which is indicative of cluster formation and relative cluster size. The results are then normalized based on the actual nanotube results.

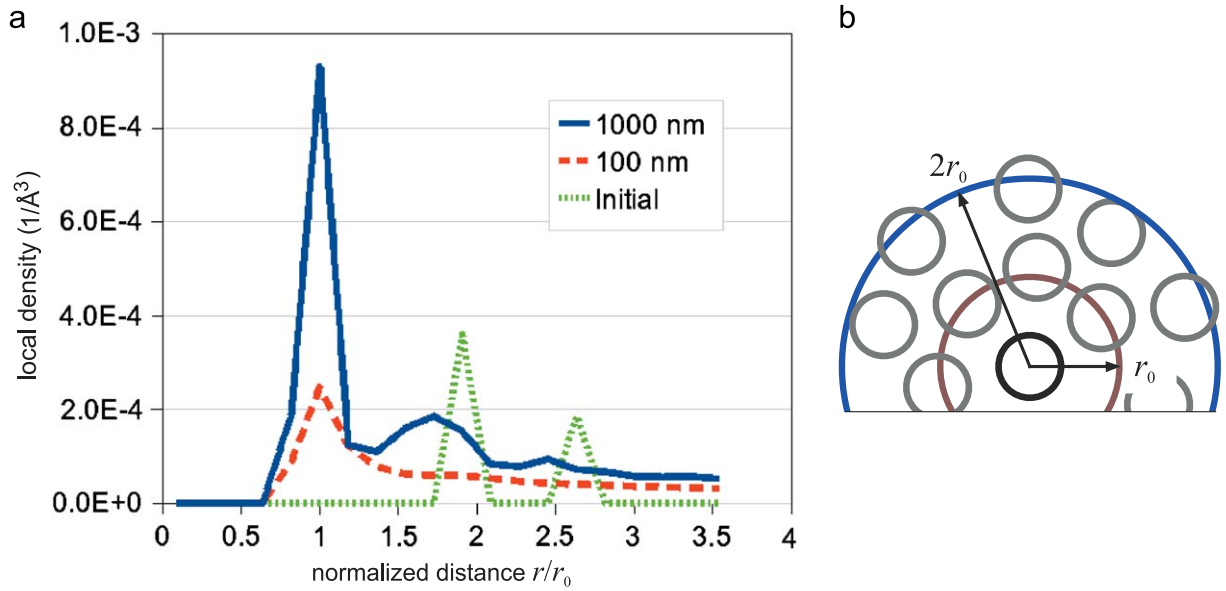


Fig. 11. (a) Local density distributions for CNTs of length 100 nm (Example 1) and 1000 nm (Example 2), for SWCNT simulations. (b) Schematic of local density distribution.

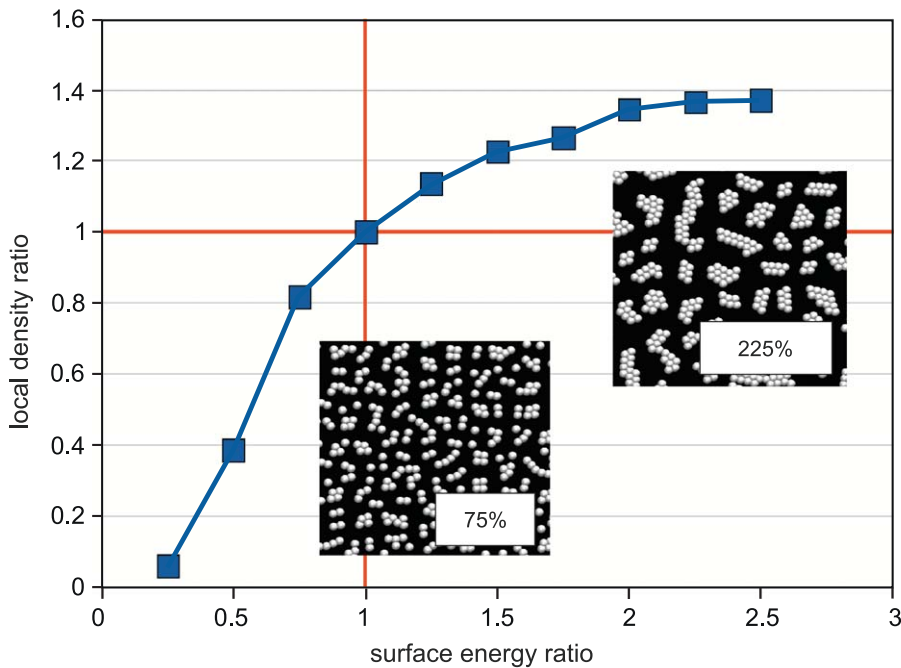


Fig. 12. Normalized peak local densities versus surface energy ratio for 1000 nm array of (5,5) SWCNT; surface energy values from 25% to 250% actual value of 2.31×10^{-10} J/m. Peak local density at equilibrium spacing of approximately 10.5 Å. Insets depict top view of array clusters at 75% and 225% values. The density saturates as surface energy approaches 250% actual value, as a significant decrease in van der Waals forces with distance prevents attraction of next-nearest neighbors.

As shown in Fig. 12, decreasing the surface energy effectively ceases the formation of bundles or clusters, reducing the attraction between adjacent tubes such that resistance due to bending stiffness is dominant. Increasing the surface energy causes an increase in cluster size, but reaches a saturation point. Increasing the surface energy 200% to 250% only increases the local density by approximately 30%. This saturation occurs due to the relatively short range of the peak of van der Waals forces. The forces due to long-range interactions decay quickly, and the tubes are tightly bonded in clusters at high surface energy. The spacing between each cluster is too great a distance to attract the next nearest tubes, which are

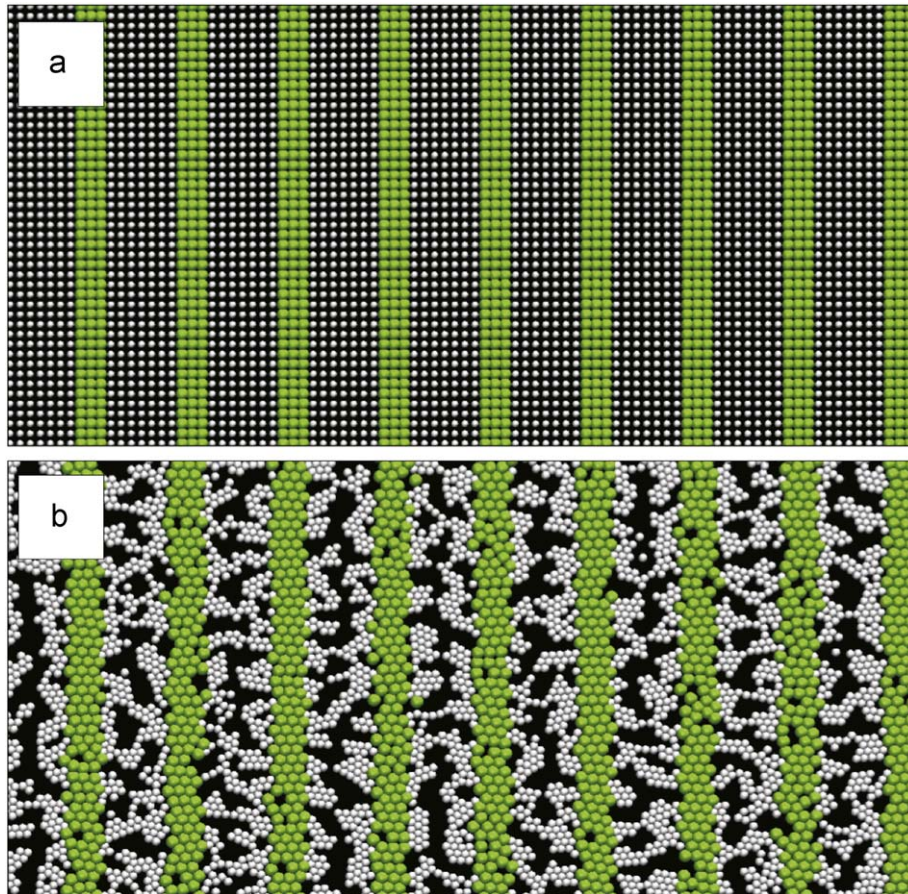


Fig. 13. Heterogeneous array of SWCNTs (aspect ratio=1500, in white) and DWCNTs (aspect ratio=625, in green); dimensions: approx. $0.2 \mu\text{m} \times 0.1 \mu\text{m}$. (a) Initial configuration. (b) Bundled configuration. This result shows that the utilization of heterogeneous arrays can be employed to intentionally manipulate the bundle density and configuration to form specific surface structures. (For interpretation of the references to color in this figure legend, the reader is referred to the web version of this article.)

strongly adhered to other formed clusters. The maximum cluster size then becomes dependent on the initial geometry of the array (such as nanotube spacing and density) and nanotube properties (aspect ratio and bending stiffness).

4.5. Example 3: large aspect ratio mixed arrays

An array of mixed carbon nanotubes (both SWCNT and DWCNT) is generated with alternating strips of DWCNTs. Again each “lollipop” nanotube model is 1000 nm in height, a spacing of 20 \AA in each direction center-to-center, and periodic boundary conditions. Due to the increase in diameter, the DWCNT has a lower aspect ratio (approx. 625), but an increase in surface energy and thus attraction to adjacent nanotubes. Further, the bending stiffness of the DWCNTs is an order of magnitude greater than the SWCNTs (see Table 3). Essentially, the stiffer, more energetic DWCNTs attract the SWCNTs, creating bands of dense nanotube bundles (Fig. 13).

It is noted that the initial 20 \AA spacing is approximately the equilibrium spacing of the DWCNTs, which consequently maintain their initial “striped” patterning.

5. Discussion and conclusion

An understanding of the structure–property relationship at the meso- and macro-scale constitute a fundamental challenge of atomistic and molecular investigations of materials due to inherent limitations of both time and length scales. The concept of reducing a complex system to a minimal number of degrees of freedom is a common practice in structural engineering, ranging from nodal analysis of moment frames (McGuire et al., 2000) to lumped-mass idealizations for seismic engineering (Chopra, 2000). The approach is intended to provide an efficient means for first-order analysis and

design, providing the foundation for more comprehensive analysis. The inherent complexity of molecular systems such as an array of carbon nanotubes or other complex systems promotes and necessitates such simplifications. The importance of the interaction and the consequential bundling of nanotubes at the atomistic, molecular, and global material scales are critical for the development of materials and systems taking advantage of the surface characteristics of such arrays. Pertinent behaviors such as field emission properties (Fan et al., 1999), thermal conductivity (Shaikh et al., 2007), and array-substrate adhesion (Qu et al., 2008) could possibly be coupled to this simplified model, enabling efficient simulations, optimization, and/or first-order designs.

The single-degree-of-freedom model is meant to reduce the effective mechanical behavior of a nanotube to the fewest parameters possible, for efficient molecular dynamic simulations, representing a “coarse-graining” approach in the superlative sense. It is noted that a simplified modeling technique is not capable of reproducing detailed atomic and nanoscale behavior of carbon nanotube arrays, but such behavior is not the goal. Rather, the current model is intended for large-scale modeling of bundling. The simple “lollipop” model reported here opens up several possibilities for future studies, including surface patterning, and/or transmission phenomena (such as thermal or electrical conductivity). Further, the SDOF approach can possibly be applied to other “self-similar” systems (in the sense of consistent interactions between system components), extending the time and length scales of effective molecular dynamic investigations.

In general, theoretical nanomechanical models similar to those described for nanotube adhesion can be implemented in other high-aspect-ratio nanostructural arrays wherein bundling and inter-tube attraction is not of critical concern. Such simplification techniques could theoretically be utilized for an assortment of nanotube phenomena, including arrays with mechanomutable or magnetically active surface properties (Cranford and Buehler, 2009; Evans et al., 2007), or nanotube assemblies implemented for sensing applications (Artzi-Gerlitz et al., 2009; Dai et al., 2002; Dijkstra et al., 2005; Sotiropoulou and Chaniotakis, 2003), or other systems that can be elucidated by *global* rather than *local* behavior of individual nanotubes.

An understanding of the effects of surface energy and cluster formation can facilitate the development of devices that attempt to manipulate the energy and inter-tube interaction of nanotubes, including nanotube actuators (Baughman et al., 1999) or computing devices (Rueckes et al., 2000). Further, such phenomenon occurs in general in nanotube arrays of other materials, such as polymer nanofilaments (Linares et al., 2009), or polymer-coated composite nanotubes (Star et al., 2001). The current model framework can also be implemented to investigate the environmental effects on surface energy and bundle formation, such as changes in pH for nanotube arrays (or free nanotubes) in solution (Saleh et al., 2008), or the energetic effects of the nanotube–substrate interface. We have shown that although surface energy is critical for the attraction of adjacent nanotubes, cluster density reaches a saturation point based on the initial geometry and mechanical properties of individual nanotubes. Understanding of such behavior is critical in the development of novel nanotube displays (Wang et al., 1998) and electronic devices (Li et al., 1999; Murakami et al., 2000) that depend on the ordered arrangement and density of such arrays.

The system level behavior of nanotube systems is a complex problem, involving a tacit accord between surface density, height, spatial arrangement, and other parameters. Here we have focused on relatively homogeneous arrays to validate our nanomechanical model, as well as manipulating surface energy to determine the effect on cluster formation. Future areas to study could be heterogeneity in surface density and height, and geometric spatial arrangement, as well as incorporating the potential modification/manipulation of surface energy *in situ*.

In summary, we derived a continuum model for the relation between elastic energy (via bending stiffness) and intermolecular interaction energy for carbon nanotubes, resulting in a prediction of the required bent and contact lengths of a pair of adjacent nanotubes at equilibrium. The model was confirmed via coarse-grain molecular simulations implementing a bead–spring representation of carbon nanotubes. A single-degree-of-freedom “lollipop” model was developed from the continuum theory and parameters obtained from full atomistic simulations. The approach is fundamentally multi-scale, and provides a new technique for the simulation and investigation of arrays of carbon nanotubes approaching length-scales of micrometers, greater than traditional molecular dynamics or current coarse-grain techniques.

The bundle formation of carbon nanotubes involves a balance between surface energy, inter-tube spacing, bending stiffness, and aspect ratio. Deliberate manipulation of each parameter can manipulate the final configuration of a nanotube array. It has been illustrated that changes in nanotube length affect cluster density, while mixing of single-walled carbon nanotubes with stiffer, double-walled carbon nanotubes illustrated a propensity for regular patterns. Subsequently, one can alter the self-organization of nanotube arrays with design and intent. Effective simulation methods are critical when the self-assembly process of the system is inherently stochastic. The single degree of freedom “lollipop” model presented here provides an efficient means to engineer the self-organization and principal behavior of nanotube arrays.

Acknowledgements

This work was supported primarily by the MRSEC Program of the National Science Foundation under award number DMR-0819762. The calculations and the analysis were carried out using a parallelized LINUX cluster at MIT’s Atomistic

Mechanics Modeling Laboratory. Visualization has been carried out using the VMD visualization package (Humphrey et al., 1996).

References

- Ajayan, P.M., Banhart, F., 2002. Strong bundles. *Nature Materials* 3, 135–136.
- Al-Haik, M., Hussaini, M.Y., Garmestani, H., 2005. Adhesion energy in carbon nanotube-polyethylene composite: effect of chirality. *Journal of Applied Physics* 97 (7), 074306.
- Artzi-Gerlitz, R., Benkstein, K.D., Lahr, D.L., Hertz, J.L., Montgomery, C.B., Bonevich, J.E., Semancik, S., Tarlov, M.J., 2009. Fabrication and gas sensing performance of parallel assemblies of metal oxide nanotubes supported by porous aluminum oxide membranes. *Sensors and Actuators B: Chemical* 136, 257–264.
- Baughman, R.H., Cui, C., Zakhidov, A.A., Iqbal, Z., Barisci, J.N., Spinks, G.M., Wallace, G.G., 1999. Carbon nanotube actuators. *Science* 284, 1340.
- Baughman, R.H., Zakhidov, A.A., de Heer, W.A., 2002. Carbon nanotubes—the route toward applications. *Science* 297, 787–792.
- Brenner, D.W., Robertson, D.H., Elert, M.L., White, T.C., 1993. Detonations at nanometer resolution using molecular dynamics. *Physical Review Letters* 70, 2174–2177.
- Bronikowski, M., 2006. CVD growth of carbon nanotube bundle arrays. *Carbon* 44, 2822–2832.
- Buehler, M.J., 2006. Mesoscale modeling of mechanics of carbon nanotubes: self-assembly, self-folding, and fracture. *Journal of Materials Research* 21 (11), 2855–2869.
- Cetin, A., Kalkanli, A., 2009. Multi-scale characterization of particle clustering in discontinuously reinforced composites. *Materials Characterization* 60, 568–572.
- Chen, B., Gao, M., Zuo, J.M., Qu, S., Liu, B., Huang, Y., 2003. Binding energy of parallel carbon nanotubes. *Applied Physics Letters* 83 (17).
- Chopra, A.K., 2000. *Dynamics of Structures: Theory and Applications to Earthquake Engineering*, second edition Prentice Hall, New Jersey.
- Cranford, S., Buehler, M.J., 2009. Mechanomutable carbon nanotube arrays. *International Journal of Materials and Structural Integrity* 3 (2–3), 161–178.
- Cranford, S., Sen, D., Buehler, M.J., 2009. Meso-origami: folding multilayer graphene sheets. *Applied Physics Letters* 95, 123121.
- Dai, L., Soundarrajan, P., Kim, T., 2002. Sensors and sensor arrays based on conjugated polymers and carbon nanotubes. *Pure and Applied Chemistry* 74 (9), 1753–1772.
- Dalton, A.B., Collins, S., Munoz, E., Razal, J.M., Ebron, V.H., Ferraris, J.P., Coleman, J.N., Kim, B.G., Baughman, R.H., 2003. Super-tough carbon-nanotube fibers. *Nature* 423, 703.
- Dijkstra, M., van Baar, J.J., Wiegerink, R.J., Lammerink, T.S.J., de Boer, J.H., Krijnen, G.J.M., 2005. Artificial sensory hairs based on the flow sensitive receptor hairs of crickets. *Journal of Micromechanics and Microengineering* 15, S132–S138.
- Evans, B.A., Shields, A.R., Carroll, R.L., Washburn, S., Falvo, M.R., Superfine, R., 2007. Magnetically actuated nanorod arrays as biomimetic cilia. *Nano Letters* 7 (5), 1428–1434.
- Fan, S., Chapline, M.G., Franklin, N.R., Tomblor, T.W., Cassell, A.M., Dai, H., 1999. Self-oriented regular arrays of carbon nanotubes and their field emission properties. *Science* 283, 512–514.
- Glassmaker, N.J., Jagota, A., Hui, C.Y., Kim, J., 2004. Design of biomimetic fibrillar interfaces: 1. Making contact. *Journal of Royal Society London Interface* 1, 23–33.
- Hoover, W.G., 1985. Canonical dynamics: equilibrium phase-space distributions. *Physical Review A* 31 (3), 1695–1697.
- Hui, C.Y., Jagota, A., Lin, Y.Y., Kramer, E.J., 2002. Constraints on microcontact printing imposed by stamp deformation. *Langmuir* 18 (4), 1394–1407.
- Humphrey, W., Dalke, A., Schulten, K., 1996. VMD: visual molecular dynamics. *Journal of Molecular Graphics* 14 (33).
- Kis, A., Csanyi, G., Salvetat, J.P., Lee, T.N., Couteau, E., Kulik, A.J., Benoit, W., Brugger, J., Forro, L., 2004. Reinforcement of single-walled carbon nanotube bundles by intertube bridging. *Nature Materials* 3.
- Li, D.-C., Dai, L., Huang, S., Mau, A.W.H., Wang, Z.L., 2000. Structure and growth of aligned carbon nanotube films by pyrolysis. *Chemical Physics Letters* 316, 349–355.
- Li, F., Cheng, H.M., Bai, S., Su, G., Dresselhaus, M.S., 2000. Tensile strength of single-walled carbon nanotubes directly measured from their macroscopic ropes. *Applied Physics Letters* 77 (20), 3161–3163.
- Li, J., Papadopoulos, C., Xu, J.M., Moskovits, M., 1999. Highly-ordered carbon nanotube arrays for electronics applications. *Applied Physics Letters* 73 (3), 367–369.
- Liew, K.M., Wong, C.H., Tan, M.J., 2005. Buckling properties of carbon nanotubes. *Applied Physics Letters* 87 (4).
- Liew, K.M., Wong, C.H., Tan, M.J., 2006. Tensile and compressive properties of carbon nanotube bundles. *Acta Materialia* 54, 225–231.
- Linares, A.V., et al., 2009. Polymer films composed of surface-bound nanofilaments with high aspect ratios, molecularly imprinted with small molecules and proteins. *Advanced Functional Materials* 19, 1299–1303.
- Liu, X., Baronian, K.H.R., Downard, A., 2008. Patterned arrays of vertically aligned carbon nanotube microelectrodes on carbon films prepared by thermal chemical vapor deposition. *Analytical Chemistry* 80, 8835–8839.
- McGuire, W., Gallagher, R.H., Ziemian, R.D., 2000. *Matrix Structural Analysis*, second edition John Wiley and Sons, Inc., New York.
- Murakami, H., Hirakawa, M., Tanaka, C., Yamakawa, H., 2000. Field emission from well-aligned, patterned, carbon nanotube emitters. *Applied Physics Letters* 76 (13), 1776–1778.
- Plimpton, S.J., 1995. Fast parallel algorithms for short-range molecular dynamics. *Journal of Computational Physics* 117, 1–19.
- Prodanov, D., Nagelkerke, N., Marani, E., 2007. Spatial clustering in neuroanatomy: applications of different approaches to motor nerve fiber distribution. *Journal of Neuroscience Methods* 160, 93–108.
- Qi, H.J., Teo, K.B.K., Lau, K.K.S., Boyce, M.C., Milne, W.I., Robertson, J., Gleason, K.K., 2003. Determination of mechanical properties of carbon nanotubes and vertically aligned carbon nanotube forests using nanoindentation. *Journal of Mechanics and Physics of Solids* 51, 2213–2237.
- Qu, L., Dai, L., Stone, M., Xia, Z., Wang, Z.L., 2008. Carbon nanotube arrays with strong shear binding-on and easy normal lifting-off. *Science* 322, 238–242.
- Rueckes, T., Kim, K., Joselevich, E., Tseng, G.Y., Cheung, C.L., Lieber, C.M., 2000. Carbon nanotube-based nonvolatile random access memory for molecular computing. *Science* 289, 94–97.
- Saleh, N.B., Pfefferle, L.D., Elimelech, M., 2008. Aggregation kinetics of multiwalled carbon nanotubes in aquatic systems: measurements and environmental implications. *Environmental Science and Technology* 42, 7963–7969.
- Scalon, J.D., Fieller, N.R.J., Stillman, E.C., Atkinson, H.V., 2003. Spatial pattern analysis of second-phase particles in composite materials. *Materials Science Engineering A* 356, 245–257.
- Shaikh, S., Li, L., Lafdi, K., Huie, J., 2007. Thermal conductivity of an aligned carbon nanotube array. *Carbon* 45, 2608–2613.
- Sotiropoulou, S., Chaniotakis, N.A., 2003. Carbon nanotube array-based biosensor. *Analytical and Bioanalytical Chemistry* 375, 103–105.
- Star, A., Stoddart, J.F., Steuerman, D., Diehl, M., Boukai, A., Wong, E.W., Yang, X., Chung, S.-W., Choi, H., Heath, J.R., 2001. Preparation and properties of polymer-wrapped single walled carbon nanotubes. *Angewandte Chemie* 113 (9), 1771–1775.
- Steinhart, M., Wendorff, J.H., Greiner, A., Wehrspohn, R.B., Nielsch, K., Schilling, J., Choi, J., Gosele, U., 2002. Polymer nanotubes by wetting of ordered porous templates. *Science* 296 (5575), 1997.
- Timoshenko, S., Macculough, G.H., 1940. *Elements of Strength of Materials*, second edition D. Van Nostrand Company, Inc., New York.
- Treacy, M.M.J., Ebbesen, T.W., Gibson, J.M., 1996. Exceptionally high Young's modulus observed for individual carbon nanotubes. *Nature* 381, 678–680.

- Wang, Q.H., Setlur, A.A., Lauerhaas, J.M., Dai, J.Y., Seelig, E.W., Chang, R.P.H., 1998. A nanotube-based field-emission flat panel display. *Applied Physics Letters* 72 (22), 2912–2913.
- Zhang, Q., Huang, J.-Q., Zhao, M.-Q., Qian, W.-Z., Wang, Y., Wei, F., 2008. Radial growth of vertically aligned carbon nanotube arrays from ethylene on ceramic spheres. *Carbon* 46 (8), 1152–1158.
- Zhou, W., Huang, Y., Liu, B., Hwang, K.C., Zuo, J.M., Buehler, M.J., Gao, H., 2007. Self-folding of single- and multi-wall carbon nanotubes. *Applied Physics Letters* 90 (073107).
- Zhu, C., Xie, Z., Guo, K., 2004. Formation of close-packed multi-wall carbon nanotube bundles. *Diamond and Related Materials* 13, 180–183.
- Zhu, H.W., Xu, C.L., Wu, D.H., Wei, B.Q., Vajtai, R., Ajayan, P.M., 2002. Direct synthesis of long single-walled carbon nanotube strands. *Science* 296, 884–886.